

A Detailed Study of Plastic Scintillating Strips with Axial Wavelength Shifting Fiber and VLPC Readout

M. Adams^a, N. Amos^b, D.A. Averill^a, P. Baringer^{b,1},
M. Chung^a, F. Hsieh^b, H. Li^c, D. Lincoln^b, S. Margulies^a,
H. Neal^b, E. Neis^b, L. Oesch^b, J. Qian^b, M. Rijssenbeek^c,
T. Yasuda^d

^a *University of Illinois at Chicago, Chicago, Illinois 60607, USA*

^b *University of Michigan, Ann Arbor, Michigan 48109, USA*

^c *State University of New York, Stony Brook, New York 11794, USA*

^d *Northeastern University, Boston, Massachusetts 02115, USA*

(for the DØ Collaboration)

The physical properties of a plastic scintillating strip with axial wavelength shifting fiber and VLPC readout have been extensively investigated. Different construction techniques were tried and eighteen variations on the basic detector were studied in a cosmic ray test stand. Over 15 000 cosmic rays were recorded per scintillating strip. The high event statistics and the greatly improved photo-statistics provided by the VLPC readout allowed us to study the system in much more detail than has been done previously. Results on light yields, signal uniformity, attenuation length, edge effects, and crosstalk are presented. Typical light yields were 18 photons per mm of scintillator traversed for minimum ionizing particles. The detectors had very uniform response at different positions along the strip.

Submitted to Nuclear Instruments and Methods in Physics Research,
Section A

¹ Visitor from *University of Kansas, Lawrence, Kansas 66045, USA*

1 Introduction

Plastic scintillator, with embedded wavelength shifting fiber (WLS) readout, has been shown to be a very efficient way to sample and measure energy loss from charged particles. This technique is often used in applications (e.g. calorimeters) where a large area needs to be covered with minimal dead regions caused by light transport. In addition, scintillating fibers are quickly becoming a very popular detector technology, used both for tracking applications as well as in the manufacture of compact calorimeters. Both of these technologies are quite mature (cf. references [1,2], and the references contained therein) and supply solutions to a vast range of technical problems.

There is a middle ground between these technologies. This is the region where relatively fine segmentation is needed, but (a) the high channel count of a scintillating fiber detector is both prohibitively expensive and unnecessary, and (b) the granularity available from conventional scintillator-WLS fiber designs is insufficient. Plastic scintillating strips with wavelength shifting fiber readout blend the salient ideas of both technologies and provide an answer to situations where light needs to be efficiently collected from long, narrow regions. They thus make an ideal candidate for a preshower detector being planned for an upgrade of the DØ detector at Fermilab. We have constructed and studied prototype detectors where the signal was brought out from the scintillating fiber through long clear fibers to Visible Light Photon Counters (VLPC's).² Our prototypes have been extensively tested in a cosmic ray stand. The large photostatistics afforded by the VLPC's and the large number of cosmic ray events collected enabled us to make a detailed study of the properties of these detectors, which we present here.

The DØ collaboration at Fermilab is presently preparing for a major detector upgrade [4], scheduled to be in place for Run II at the Tevatron. Among many other improvements, this upgrade includes removal and replacement of the entire central tracking system and installation of a solenoidal magnet with a two Tesla magnetic field. The preshower detector is designed to work together with the central tracking system and the electromagnetic calorimeter to aid in particle identification and energy resolution. The preshower will substantially assist in low- p_{\perp} electron identification (both at the trigger level and in offline reconstruction) which will improve DØ's overall b tagging capabilities—an important requirement for a number of physics topics. In addition, Monte Carlo studies [5] have shown that a scintillator preshower detector, placed on

² VLPC's are very high quantum efficiency photodetectors ($\sim 65\%$ at 530 nm) developed by Rockwell International [3]. It is expected that quantum efficiencies of 80% will soon be attained. This should be compared to the 8-15% quantum efficiencies observed for typical phototubes at WLS wavelengths.

the outside of the solenoidal magnet, will improve the electromagnetic energy resolution. While the current DØ detector [6] has exceptional electromagnetic energy resolution, this resolution would be degraded by the one radiation length of additional material (at $\theta = 90^\circ$ with respect to the beam direction) that makes up the solenoid. The preshower detector restores the current energy resolution by sampling showers after the solenoid and before the existing calorimeter.

While the details of the preshower detector design are not yet fully determined, the overall strategy is firm. Several layers of scintillator strips will be placed on the outside of the solenoidal magnet at a radius of about 75 cm. The prototype module discussed in this paper anticipates a design that uses strips with a square cross section and approximate dimensions ($2300 \times 5 \times 5$) mm. Other shapes with different cross sections (such as triangles) are being considered but are not discussed here. Wavelength shifting fibers are run in long holes along the axis of the scintillator strips. The innermost layer will have the strips aligned parallel to the cylindrical magnet's axis (i.e. the beam direction). Then two layers will be placed at a stereo angle relative to the axial strips. This angle is not yet chosen, but will either be 90° or some small angle on the order of 20° . In the event that a small stereo angle is chosen, it is likely that both u and v (e.g. $\pm 20^\circ$) layers will be present. It is possible that there will also be a second axial layer to guard against dead spaces between adjacent scintillating strips. The resulting cylindrical geometry, possibly employing helical strips, presents interesting challenges in mechanical design. This article discusses the construction and optical test results of a prototype module.

Two methods of making adjacent strips are currently under consideration. The first, called the megatile option, consists of strips created by milling grooves into a large sheet of scintillator. Adjacent grooves are cut almost completely through the sheet, leaving a small thickness of scintillator at the bottom. These grooves are then filled with an opaque, reflective, white glue. The hole for the fibers is created by using a ball-end mill to cut a groove of circular cross-section along the axis of the strips. The second method, called the extrusion option, is manufactured by extruding long individual scintillator strips with a hole at the center of the strip. In both cases, the mismatch between the cylindrical geometry of the final design and the planar geometry of scintillator strips and sheets require that strips be bent. Since the bending will either (a) introduce a stress to the plastic or (b) require that the plastic be heated to release this stress, this suggests that one must investigate the effect of heating and crazing on light output.

There are many small variations in manufacturing techniques that can be imagined. In this article we discuss several options that we chose to test. Our current results primarily explore variations in the megatile option. Preparations for similar tests of extruded scintillator are currently underway and those

results will be the subject of a subsequent article.

2 Test Stand

A principal component of the upgraded DØ detector is a scintillating fiber central tracker consisting of 80 000 scintillating fibers arranged on 4 cylinders of different radii. These fibers will be connected via clear fibers (eight meters long) to VLPC's.

Because of the daunting size and complexity of the project, the DØ Fiber Tracking Group built a cosmic ray test stand to demonstrate that a large scale system using their proposed design could be made to work. Details of the test stand are given in [7], but briefly it can be described as follows.

Figure 1 is a schematic of the test stand. Four scintillating paddles at various vertical positions provide the trigger for the apparatus. In addition, two thick steel absorbers (0.8 m and 1.4 m respectively) are stacked and separated by a several inch gap. The narrower of the paddles are placed above the steel and surround the fiber tracker group's prototype module. These paddles provide spatial constraints on the cosmic rays which are accepted. A third paddle is placed between the steel absorbers and the fourth is placed beneath both steel blocks. These paddles place energy constraints on the cosmic ray muons seen. By requiring that either three or all four paddles fired, it is possible to put a lower threshold on the energy of the cosmic ray from the known dE/dx loss in the steel.

In addition to the trigger scintillator paddles, three planes of Iarocci tubes were used: two above the steel, straddling the fiber tracker prototype, and the third between the two steel absorbers. These planes were used initially to crudely determine the position of the track. Although subsequent understanding of the fiber tracker prototype has rendered the Iarocci tubes obsolete for one view (xy), they still provide useful position information in the yz view. (The y direction is up, the z direction runs parallel to the fibers and points away from the readout end, and the x direction is chosen to make a right-handed coordinate system).

The fiber tracker prototype is composed of ribbons of 835 μm -diameter scintillating fibers, arranged into three groups of layers as shown in Fig. 1. Different ribbons are aligned either parallel to the z axis or at a small stereo angle (2°). The axial (but not the stereo) planes are used in this analysis. Therefore, the x position is determined by the fiber tracker prototype, but the z position is determined by the Iarocci planes. Consequently the x intercept is determined much more precisely than the z intercept.

Each fiber of the tracker prototype is a three meter long scintillating fiber of Kuraray [8] manufacture, containing 1% p-terphenyl and 1500 ppm 3-hydroxyflavone (3HF) [9]. Only the central two meters of fiber were in the fiducial volume of the detector. The light from each scintillating fiber is transported via an eight meter clear fiber to an individual VLPC pixel. The fiber tracker prototype consists of 3072 channels.

While the fiber tracker prototype is a technical tour de force in its own right, from the point of view of testing the preshower prototype, it is merely a very precise device for determining the trajectory and minimum energy of cosmic ray tracks. In the interest of conciseness, for the remainder of the paper we do not distinguish between information determined using the fiber tracker sub-detector and information determined using Iarocci planes. We simply call the entire track-measuring system the “fiber tracker.” The position resolution of the x coordinate is $80\text{ }\mu\text{m}$ at all values of z at the preshower prototype, and the track resolution of the z position is 3.0 mm at all values of x . The minimum track energy is 0.9 GeV and 2.5 GeV for three and four scintillators hit, respectively.

Space constraints required that the preshower prototype module be placed underneath the fiber tracker prototype, but above the steel absorbers. See Fig. 1 for details.

3 Detector Variations

Before determining our final detector design, we intend to test many small variations of the baseline design. Here we study variations on the almost square (e.g. $4.5 \times 5.0\text{ mm}$) cross section strip design which has been used by other groups [2]. After discussions with representatives from various companies, two types of Bicron [10] scintillator (BC-404A and BC-404BL) were chosen on the basis of reported light yield and reasonable cost. Both scintillators are doped with the same fluors as Bicron BC-404, although at lower concentrations. In addition, BC-404BL is a cross-linked polyvinyltoluene plastic, which improves its mechanical properties [11]. Stringent tests of these two scintillator types were performed.

Design considerations³ suggested that each strip be 4.5 mm thick and $\sim 5\text{ mm}$ wide. Wavelength shifting fiber of the type we chose to test (Kuraray Y11 [12], with K27 as the dye) was commercially available with a diameter of 0.835 mm .

³ The strips are made as thick as they can be within the allowed space budget for the final detector and the width is governed by matching the position resolution to that of the central fiber tracker.

mm. Constraints from the pre-existing D \emptyset cosmic ray test stand limited us to 128 channels and about 8 cm of transverse space. These constraints led to the following design.

Seven pieces of scintillator ($1000 \times 4.5 \times 80$) mm were manufactured. Each piece had 15 grooves milled in it, yielding 16 strips. Each detector variation used eight adjacent strips, for a total of 14 designs.

We describe here the “normal” megatile design. In each 4.5 mm thick sheet of scintillator, deep grooves were cut with a center-to-center spacing of 5 mm (0.200”). Due to variations in the thickness of the scintillator, the amount of material left at the bottom of the groove varied, but was typically 0.010”–0.020” (250–500 μm). A 0.030” (750 μm) straight bit was used to cut these grooves, which are called *isolation grooves*. These grooves were then filled with an opaque, highly reflective, white glue which was allowed to dry. A second set of grooves were cut midway between the isolation grooves (again with a 5 mm center-to-center spacing). These grooves were cut with a 0.030” straight bit to a depth of 0.060” (1.5 mm). The bit was then changed for a 0.040” (1 mm) ball cutter and a hole for the fiber was cut. The depth of the cut was set such that the bottom edge of the ball was 0.060” (1.5 mm) below the surface of the scintillator (see Fig. 2). These grooves are called *fiber grooves*.

Including the “normal” design, 14 different detector variations were investigated and are listed below. Each detector variant was carefully chosen to allow one to isolate the effect of each change. “Normal” designs were made with both types of scintillator and each variant has a single difference from one of these “normal” detectors. Unless otherwise specifically stated, all scintillator is BC-404BL and all fiber is Kuraray double clad Y11 250 ppm. The variations tested are:

404B Normal BC-404BL scintillator, manufactured normally.

404A Normal BC-404A scintillator, manufactured normally.

404B Heated BC-404BL scintillator, manufactured normally and then heated to $\sim 225^\circ$ F for approximately 30 minutes.

404A Heated BC-404A scintillator, manufactured normally and then heated to $\sim 225^\circ$ F for approximately 30 minutes.

404B Crazed BC-404BL scintillator, manufactured normally and then made to craze.

404A Crazed BC-404A scintillator, manufactured normally and then made to craze.

0.100” Normal manufacture, except the depth of the ball groove was 0.100” (2.5 mm) instead of 0.060” (1.5 mm)

0.050” Normal manufacture, except the depth of the ball groove was 0.050” (1.25 mm) instead of 0.060” (1.5 mm)

0.038” Normal manufacture, except the diameter of the ball cutter was 0.038”

(0.965 mm) rather than 0.040" (1 mm)

Black Stripe Normal manufacture, except a thin black stripe was drawn on the scintillator surface, directly beneath the isolation groove glue.

Optical Glue Normal manufacture, except after the WLS fiber was inserted, BC-600 optical glue was injected into the fiber groove, replacing the normal air gap. This kept the index of refraction approximately constant as the light travels from the scintillator, through the gap and into the fiber.

BCF-91A Normal manufacture, except single clad Bicron BCF-91A fiber (0.835 mm) was used.

Y11 350 Normal manufacture, except the dopant in the fiber was Y11 350 ppm, rather than the normal 250 ppm.

3HF Normal manufacture, except the dopants in the WLS fiber were 1% p-terphenyl and 3HF [9] at a concentration of 1500 ppm.

The megatile manufacturing variations occupied 112 of 128 available channels, or seven of eight available layers. The final layer was reserved for very preliminary tests of the extruded scintillator option. Strips of scintillator ($5 \times 5 \times 1000$) mm with a 1-mm-diameter axial hole were obtained from the Particle Detector Group at Fermilab. This scintillator had been prepared by Fermilab staff and consisted of a polystyrene base and scintillating dopants which give fluorescence spectra and light yield similar to Kuraray SCSN-81 [13]. As before, Kuraray Y11 250 ppm double-clad fibers are used.

Because only 16 channels were available to test the extruded option, it was decided to make four extrusion variants of four strips each. These variations were called:

Normal Extruded Two parallel sides (5×1000) mm were carefully painted white. The remaining two sides were left bare. This variation was designed to have a reflection geometry similar to the megatile design.

Clear Extruded Strips were left bare (i.e. no surface preparation).

White Extruded Strip surfaces were entirely painted with a glossy white latex paint.

Black Extruded Strip surfaces were entirely painted with a flat black latex paint.

4 Prototype Construction

4.1 Megatile Construction Details

The megatiles were cut at Fermilab. A ($1524 \times 610 \times 4.5$) mm sheet of BC-404BL was placed on a Thermwood milling machine (a computer controlled

precision mill) and isolation grooves sufficient for seven megatiles, each consisting of 16 strips, were cut. Prior to cutting, the protective films were removed from both sides of the scintillator. The megatiles were not cut from the parent scintillator sheet at this time; only the isolation grooves were cut. Each isolation groove was 102 cm long. In addition, alignment holes were cut. This construction stage took approximately eight hours. The scintillator was then removed from the milling machine. The isolation grooves made the remaining scintillator very flimsy, so extreme care was necessary.

The next stage in megatile manufacturing was the injection of the isolation glue. The glue formula and techniques of glue injection were taken largely from CDF's endcap upgrade efforts and are given in exhaustive detail in [14]. Briefly, the surface of the scintillator with the open grooves was thoroughly cleaned with ethanol and the grooves were inspected to ensure that all debris from the cutting stage had been removed. Four-inch wide Kapton tape was laid in adjacent strips over the open grooves. A roller aided in giving good contact between the Kapton and the scintillator. Three small holes were made in the Kapton for each groove, one in the center and one at each end. White isolation glue⁴ was injected into the center hole via a pneumatic hypodermic. The end holes served as vents, allowing the glue to flow to the ends. After each groove was filled, the holes were covered and the next groove was filled. For reasons that will be given later, certain grooves were not filled. After the grooves had been filled, the tile was allowed to cure at room temperature for several days. The tile was then inspected for air bubbles in the glue and any such defects were repaired by injecting more isolation glue. After several more days of curing, the Kapton tape was carefully removed and the surface cleaned again with ethanol. This procedure, properly done, yields a clean surface with little stray glue.

The scintillator was then returned to the Thermwood milling machine and the fiber grooves cut. This was done in two stages, first cutting the fiber groove with a 0.030" (0.75 mm) straight mill, followed by a second cut with a ball-end mill (typically 0.040" (1 mm)). Special care was needed at this stage as it was at this time that the different manufacturing variations were added (different ball groove depth, different ball mill diameter, etc.).

Finally, the megatiles were cut from the parent scintillator sheet. The result was seven ($1000 \times 80 \times 4.5$) mm megatiles, each consisting of sixteen 5 mm wide strips. Each megatile contained two manufacturing variations, consisting of eight strips each. Some of these megatiles were set aside either as spares or

⁴ The isolation glue consisted of: Dow Corporation DER-332 epoxy, Dupont Corporation "Ti-Pure R700" titanium dioxide, and Texaco Corporation Jaffamine D-230 as a curing agent. These materials were mixed in the ratio (DER-332):(TiO₂):(D-230) → 100:50:32 by weight. See Ref. [14] for more details.

for radiation testing and were not included in the cosmic ray test.

The entire process was repeated with a sheet of BC-404A scintillator of the same size. The procedure was identical, except only two 16-strip megatiles were made.

Some of the detector configurations required special handling. For instance, it would not be possible to heat only eight strips of a 16-strip megatile. For this reason, two of the BC-404BL and both BC-404A megatiles did not have isolation glue injected into the center groove. This allowed each 16-strip megatile to be easily separated into two eight-strip tiles. It was then possible to manufacture each particular detector configuration. Those configurations that required additional special construction efforts were:

Heating After the isolation glue had cured, the BC-404A and BC-404BL eight-strip tiles were placed at the same time in an oven heated to 225° F for about 30 minutes. The precision of the oven thermometer calibration is unknown and the thermometer was unavoidably situated some distance from the scintillator, but it is certain that both tiles were heated enough to soften and wet the underlying surface. Neither were heated enough to have substantial permanent shape distortion.

Crazing After the isolation glue had cured, eight-strip tiles of BC-404A and BC-404BL were placed on a cylinder of 70 cm radius for a period of 1 month. In order to maximize total stress (and therefore crazing), the long axis of the tile was oriented perpendicular to the cylinder axis and strapped down (i.e. if the cylinder end is taken to be a circle, the strips were forced to follow the circle circumference). After one month, some crazing was visible on both samples, although it was much less than similar samples, identical except lacking the isolation glue, placed on the cylinder for a similar time. After removal from the cylinder, the BC-404BL sample returned to the original flat shape more quickly than the BC-404A sample.

Optical Glue After WLS fibers were inserted into the fiber grooves (details given below), a fresh layer of Kapton tape was applied to the top of the megatile. Small holes were made in the Kapton tape at the center of the fiber groove. Using the same apparatus as was used to inject white isolation glue, Bicron BC-600 (a clear, colorless optical glue, with index of refraction 1.58) was injected into the fiber groove through the holes in the Kapton tape. After the BC-600 had cured, each fiber was found to be firmly potted in the fiber groove without air bubbles. The Kapton tape was then removed.

Black Stripe The megatile was flipped so its unmilled side was facing up. Then, using a straight edge and a black magic marker, a line (approximately 0.1" wide) was drawn directly underneath each isolation groove. Special care was taken to ensure each line was truly black.

4.2 Extrusion Construction Details

Preparing the extrusions was relatively easy. The (5×5) mm cross-section strips were cut to 1 meter lengths and their ends were diamond polished. The strips were then painted. For the Black and White strips, this consisted of holding the strips vertically and spinning them around their long axis while the paint was sprayed on (all strips received two or three coats). Care must be taken to avoid uneven paint build-up (e.g. drips). Such paint non-uniformities have little effect on the optics (assuming the surface is entirely covered) but can affect how snugly the strips can fit together.

The Normal strips were more time consuming to prepare. Each strip had two sides hand painted using a small brush. The uniformity of the paint was reasonable, but noticeably worse than for the White and Black strips. If this design is chosen for the final detector, substantial R&D will be needed to improve this phase of fabrication.

4.3 Wavelength Shifting Fiber Insertion

Primarily Kuraray Y11 (250 ppm concentration) double clad fiber was used. In addition, single clad BCF-91A, double clad 3HF (1500 ppm concentration, these were spares from the fiber tracker) and double clad Y11 (350 ppm concentration) fibers were prepared.

Double clad fibers consist of a core and two layers of cladding (indices of refraction $n_{\text{core}} = 1.59$, $n_{\text{clad}1} = 1.49$, $n_{\text{clad}2} = 1.42$). Single clad fibers are of the more conventional core and single cladding construction ($n_{\text{core}} = 1.59$, $n_{\text{clad}} = 1.49$). Simple optics shows that double clad fibers give an improved light yield over single clad ones by increasing the fraction of light that undergoes total internal reflection. Double clad fibers give 70% more light, simply due to this optical effect, than comparable single clad fibers.

All fibers were 0.835 mm in diameter and cut to 1.5 m length. One end was polished and then silvered by vacuum deposition.

Each fiber was placed in the appropriate fiber groove with the silvered end flush with the end of the scintillator. Each fiber was held in place by a single drop of 5 minute epoxy at each end of the fiber groove. With the exception of the optical glue variation, in all cases there was an air gap between the scintillator and the WLS fiber.

4.4 Final Assembly

Once the scintillator had been prepared and the fibers inserted, each 16-strip megatile was wrapped in Tyvek [1,15] and placed in the final holder. In the case of the eight-strip tiles, two were placed beside one another and similarly wrapped. Positioning was determined both by (a) pins that extended through all the megatile layers and (b) by an external holder. Each layer was staggered with respect to the layer above and below (see Fig. 2) to ensure that the optically dead region caused by the isolation glue was covered by an active region in an adjacent layer.

After the prototype model had undergone final assembly, the 128 WLS fibers were inserted into the same type of optical connector used by the Fiber Tracker Group [16], potted with BC-600 optical glue, cut and polished. By using the same connector as the Fiber Tracker Group, installation of the preshower prototype was as simple as putting it in the right place, surveying it, disconnecting a layer of scintillating fiber from the fiber tracker prototype readout and replacing it with the preshower prototype connector. The smooth installation and instant functionality were surprisingly trouble free.

The signals from the preshower prototype were piped via eight-meter clear fibers to individual VLPCs. The VLPC outputs were then digitized and recorded along with the rest of the fiber tracking prototype as part of the standard data stream. The response of the VLPC is sensitive to both bias voltage and temperature [3]. For this test, the bias voltage of all VLPC pixels was 6.5 V and the temperature was held constant at 6.5 K.

5 Results of Cosmic Ray Testing

Many aspects of the performance of the preshower prototype were investigated. Properties such as spatial uniformity of response, light yields, and crosstalk are studied here.

The preshower module was installed in the test stand in mid-November 1994. During a one month run, 3.1 million triggers were accumulated. After taking into account the smaller acceptance of the preshower prototype, tracking efficiencies, and a high energy (i.e. four trigger scintillators fired) cut, 250 000 events were available for analysis, yielding approximately 16 000 events per strip.

The possible slopes of useful tracks are restricted by the triggering and track finding conditions. The distributions of the projections of the slope ($\partial x / \partial y$)

and $\partial z / \partial y$) are Gaussian-like in shape with standard deviations $\sigma_{xy} = 0.0532$ and $\sigma_{zy} = 0.288$. Thus the tracks are much more vertical in the xy projection than they are in the yz projection, as dictated by the trigger geometry.

The conversion between ADC counts and photoelectrons is done by utilizing the small amount of crosstalk seen. Using the information from the fiber tracker to determine which strips were hit, and by looking at the signal in the strips adjacent to the hit strips, one could easily see the 0, 1 and 2 photoelectron peaks. By determining the peak-to-peak separation, the ADC-to-photoelectron conversion was obtained. Figure 3 shows an example of the low number of photoelectron spectra.

The amplifier-to-ADC electronic chain was known to have a significantly nonlinear response. This nonlinearity was investigated by injecting known amounts of charge into the amplifier and plotting charge as a function of ADC counts. This ADC-to-charge calibration was converted to the ADC-to-photoelectron calibration by observing that for ADC counts corresponding to 1 or 2 photoelectrons, the charge-to-ADC calibration was linear. Simple arithmetic then allows the ADC-to-charge curve to be scaled to the more useful ADC-to-photoelectrons, by multiplying the charge axis by the charge-to-photoelectron conversion factor appropriate for low pulse height, linear behavior. Each strip was handled separately. For a typical nonlinearity curve, see Fig. 4. The curves were fit to a fourth order polynomial. For large signals, the number of photoelectrons indicated by the curve is significantly higher than that given by a linear fit to the small signal region. When a linear fit gives 10, 20 and 30 photoelectrons for a set of three signals, the curve indicates 2.0%, 7.5% and 49% more photoelectrons respectively. This illustrates the importance of using the fitted curve to make nonlinearity corrections when determining the number of photoelectrons.

While this test does not explicitly include VLPC nonlinearities, Ref. [17] and the discussion of the angle effect given in Sect. (5.3) show that the VLPC nonlinearity is not large in this region. From this point on, all results will be given in terms of pedestal subtracted, nonlinearity corrected, photoelectrons.

The first step after installation was to verify alignment. Since the preshower prototype was small enough to comfortably fit within the acceptance of the fiber tracker, the preshower prototype was placed approximately in the center of the fiber tracker and the final survey was done with tracks. As will be seen below, the signal in most strips is quite distinct from pedestal. This allowed us to require a large signal in a strip. This is equivalent to requiring that the strip be hit by a track, but does not use the fiber tracker to determine which strip is hit. We form a residual between the strip's nominal center and the track intercept position of the cosmic ray with the strip, as determined from the fiber tracker. Plotting the average residual as a function of z (position

along the strip) showed that there was a 3 mm offset and a 0.6 milliradian rotation in the xz plane. The 3 mm offset is a global offset between the surveyors coordinate system and the internal coordinate system of the fiber tracker prototype. The extruded strips were somewhat more difficult to align, since during construction their shape was deformed such that they were no longer straight. This required complicated z -dependent position corrections of the strip center for the extruded strips. After corrections, the x position of the edge of each strip was known to $\sim 50 \mu\text{m}$ for all values of z . The y position of each strip is known to less precision, typically 1 or 2 mm. The z position of the strips was determined by looking at the average signal as a function of z . At the ends of the strips, obviously the average signal goes to zero (see Sect. (5.6)). This approach allowed the z position of each strip to be known to 1 or 2 mm. The disparity in the precision of the determination of the track position in the various views reflects the resolution of the fiber tracker.

5.1 Attenuation Length

The first property to be investigated was the attenuation length, λ , of the signal in the fiber. First, a direct measurement of λ was made. A WLS fiber was attached to a photodiode and was irradiated at various positions with a point ultra-violet light source. Under these conditions, the attenuation length was determined to be (4.5 ± 0.5) meters. The relatively large uncertainty is due to the fact that the length of the fiber that was irradiated was only a small fraction of the attenuation length.

In principle, one would expect to get a more precise determination of λ from the cosmic ray data but this measurement is complicated by the fact that the fibers are silvered on one end. Without the silvering, one would expect the signal to fall as $e^{-z/\lambda}$. However, the silvering adds a second term:

$$I = I_{\circ}(e^{-z/\lambda} + Re^{-(2L-z)/\lambda}), \quad (1)$$

where I is the average signal measured as a function of z , I_{\circ} is the signal transported in one direction by the fiber, L is the length of the scintillator, and R is the reflection coefficient of the silvering.

Fitting the cosmic ray data, shown in Fig. 5, to $I = I_{\circ}e^{-z/\lambda_{\text{eff}}}$ typically gives $\lambda_{\text{eff}} = 11$ m. If one uses Eq. 1 instead, reasonable parameters (i.e. previously measured) are $\lambda = 4.5$ m, $R = 0.7$ and $L = 1$ m. This curve is difficult to distinguish from $e^{-z/\lambda_{\text{eff}}}$. Discerning between $(\lambda, R) = (4.5 \text{ m}, 0.7)$ and $(11 \text{ m}, 0.0)$ requires a 0.5% measurement, which is not possible due to systematic errors from the non-uniformity in fabrication.

The value of λ_{eff} is potentially misleading but suggestive. While this number is not a “true” attenuation length, it reflects the fact that the strip gives remarkably uniform response over its one-meter length. Since the effect of attenuation length is determined to be very small, the results of further studies integrate over all values of $10 < z < 90$ cm. The range of z covered by the preshower prototype module is $0 < z < 100$ cm.

5.2 Signal Uniformity Across Strip

The next detector property studied was the signal uniformity as a function of x position. Since each strip has a fiber groove along its axis, it is expected that the average signal would be smaller if a cosmic ray traversed the fiber (and therefore less scintillator). Examples of the data are given in Fig. 6. The gross features of the plots are easy to understand. A dip at the center is readily visible, with the size of the dip related to the depth of the fiber groove. The behavior at the edges of the strip is also easily understood from two factors. First, the center-to-center spacing of the isolation grooves is 5 mm, so the 0.8 mm width of the isolation groove places the position of the scintillator edge at ± 2.1 mm with respect to the strip center. (This position is indicated in Fig. 6.) Second, the tracks are not all vertical and there is also an uncertainty in the track position. The observed position and shape of the average signal response at the edges of the strip agrees with expectations from these considerations.

Another noticeable feature is the small asymmetry in the positioning of the central dip from the fiber groove. The offset is about 100 μm and is observed in all of the detector variations, although it is most apparent in the **0.100”** case. This offset likely resulted when the scintillator was removed from the milling machine after cutting the isolation grooves and before cutting the fiber grooves. It is thought that the scintillating sheet was not replaced exactly in its initial position when it was returned to the milling machine. Improving the reproducibility of scintillator positioning to better than 100 μm will require some effort.

To quantify the result, the ratio $R = s/S$ is defined, where s is the average signal at the center of the dip, and S is the average signal in the region of maximum signal. Table 1 divides the different detector configurations into categories and gives the ratio R . It is expected that R should be related to the depth of the fiber groove and thus the megatile data can be separated into three groups: **0.100”**, **0.050”**, and all the rest (0.060”). Further, the extrusions should have a different behavior. Certainly these expectations seem to be supported by the data. The two cases which have more than a single sample (**0.060”** and **Extruded**) seem to have a degree of uniformity in their R values. The net result is the less material removed in manufacturing the fiber

groove, the more uniform the light yield. It would seem that the R ratio should be equal to the ratio of the thickness of scintillator at the edge and the center, but this expectation neglects the fact that the amount of scintillator traversed is a function of incident angle. The data contain insufficient statistics to require only vertical tracks. The error of ± 0.01 reported in Table 1 is statistical. The scatter in the values suggests an additional systematic component to the error of ± 0.015 . These two errors should be added in quadrature.

5.3 Angle Effect

The angle effect is presented as a consistency check. Particles hit the surface of the preshower prototype at some angle θ with respect to the normal. Neglecting non-uniformities in light collection efficiency, it is expected that the signal should be proportional to the amount of scintillator traversed. We define the fractional path length, $p = \sqrt{1 + (\partial x / \partial y)^2 + (\partial z / \partial y)^2}$, where $\partial x / \partial y$ and $\partial z / \partial y$ are the one-dimensional slopes of the track. At $\theta = 0$ we have $p = 1$.

One may plot average signal, $S(\theta)$, as a function of p and fit the data with a straight line. After the fit, one may determine $S(0)$ and replot $S(\theta)/S(0)$ as a function of p and refit with a straight line. The simple ansatz given above indicates that the slope should be unity and the intercept should be zero. We observe a slope of 1.02 ± 0.02 and an intercept of -0.023 ± 0.024 . It is very important to note that when this same exercise is done without correcting for the amplifier nonlinearities, neither the slope nor the intercept is as expected. This provides confirmation that the nonlinearity of the electronics chain is being removed correctly and that the VLPC makes only a minor contribution to the overall nonlinearity.

5.4 Yield

One of the most important measurements that needs to be made is the photo-electron yield for each detector variation. Because of the non-uniform response near the groove and near the scintillator edges, data near the center and the edges are excluded. A residual (Δx) is determined, which is the distance between the track intercept and the center of the nominally hit strip. A cut excluding residuals in the regions $|\Delta x| > 1.5$ mm or $|\Delta x| < 0.5$ mm is applied. Further, each signal is divided by its fractional path length as suggested above. Finally, in order to compare the response fairly, each variation is divided by its true thickness (measured randomly and averaged). The thicknesses are 4.3 mm for BC-404A, 3.9 mm for BC-404BL, and 5.0 mm for extruded strips. The final result presented is a distribution of photoelectron yields given in

photoelectrons per mm. One should interpret this result with care, since it is heavily dependent upon geometry, but it is meaningful to compare the different detector variations. Because the shapes of the yield distributions of most detector variations are nearly the same, the results are presented in tabular form with the mean and RMS given. Figure 7 shows the shape of a typical distribution, and Table 2 tabulates the results.

The number of photoelectrons observed, while an interesting number, includes effects that do not reflect the performance of the detector itself. The detector consists of one meter long scintillator strips with 1.5 meter long axial WLS fiber with one silvered end. However, in addition, the light readout path includes other elements, each of which degrade the total signal seen. These elements are: an optical connector ($95 \pm 5\%$ transmission), eight meters of clear fiber with a 10.4 ± 0.5 meter [18] attenuation length ($46 \pm 2\%$ transmission), a second optical connector ($95 \pm 5\%$ transmission), and the *effective* quantum efficiency (QE) of the VLPC ($65 \pm 13\%$ conversion). The effective QE is a complex quantity which includes not only the conventional QE (i.e. the number of electrons produced per incident photon), but also includes other effects that affect the electron yield. For instance, a slight positioning mis-match between a fiber and the active area of a VLPC pixel, some small contaminant between the fiber and the pixel, or a blemish in the fiber or VLPC surface can all degrade the conversion of photons into electrons. Since these effects can affect the electron yield, we combine them with the conventional QE and call the final result an *effective* QE. Many of these effects are not explicitly measured, so the effective quantum efficiency is quoted to have a 20% error ($20\% = 13\%/65\%$).

When the effects of the four elements in the light readout path are combined, these elements degrade the signal by a factor of 0.272 ± 0.054 . Thus, the number of photons exiting the WLS fiber is approximately 3.68 ± 0.74 times greater than the number of photoelectrons observed.

There is an additional complication that needs to be considered. The above quoted 20% error in the effective QE reflects an uncertainty in the global QE, which affects each channel equally. Individual channels may also vary with respect to the mean behavior. This possibility was investigated by injecting the same (although unknown) amount of light into each VLPC pixel and measuring the average number of photoelectrons observed. The RMS of this variation was 11.5% although the fluctuation was not randomly distributed over the 128 VLPC pixels. Broadly speaking, eight adjacent channels have a similar response, but this might be quite different from the next eight channels. This response variation was corrected for each channel. Due to an uncertainty in the reproducibility of the light source, a systematic error of 5% was assigned to this correction. Since we average over 8 samples per detector variation, we expect that the systematic error caused by this effect for a particular preshower

detector variation is smaller ($5\%/\sqrt{8}$).

Similarly, the error reported in the connector transmission coefficient (5%) denotes the variation between individual connectors. This uncertainty is caused by slight variations in alignment (for instance the WLS fibers may not be perfectly aligned with the clear fibers). This effect is a global shift. Within a connector, each fiber is affected nearly the same. Consequently, while it is true that the actual transmission factor for the connector is known to only 5%, all of the fibers in the connector have the same light transmission to within 1%.

The treatment of errors in the yield results is subtle and warrants additional discussion. The number of photoelectrons is determined with 2% precision. The photon yield of each channel is corrected to the mean behavior to within 5%. However, the mean behavior is known only to 20%, primarily due to the global uncertainty in the effective QE. When the number of photons exiting the detector is calculated, it is thus necessary to report an error of 20%, essentially entirely due to the uncertainty in the global effective QE of the VLPCs. However, when a ratio is formed of the response of different strips (or detector variants), this error is normalized out, as it scales each channel identically. Thus one is able to compare the different detector types with a precision much better than the 20% precision obtained for the photon yields. Table 2 lists the photoelectron yields, the photon yields, and the response of the different detectors, relative to **BC-404B Normal**. It is quite apparent that the systematic effects caused by the differences in effective QE are substantial and have a non-negligible effect on the comparisons between detector variants.

The yield numbers seem to agree with expectations. For instance, the three detector variations **BC-404B Normal**, **0.050"** and **0.038"** are very nearly identical and they have light yields which agree with this expectation. Bicron Corporation claims [11] that the nominal light yields for BC-404A and BC-404BL scintillator are 59% and 63% of anthracene respectively. The expected ratio of (BC-404A)/(BC-404BL) is 94%, in agreement with our measurements.

As expected, minor variations in construction do affect light yield. The range seen, from top to bottom, is about a factor of two. In a separate test we found that the light yield of SCSN-81 is approximately $\sim 70\%$ of that seen in BC-404A and BC-404BL. In both cases, the light is first converted in Y11 WLS fibers. When one compares the extruded strip response to typical megatile response, one sees a 60% ratio. This is in fair agreement, especially considering the extruded strips are not actually SCSN-81. These observations suggest that extrusions that are manufactured to have spectral response and light yield similar to BC-404 will have response similar to that seen in megatiles.

Another interesting observation concerns the **BCF-91A** detector variation,

which has a response of 72% of the baseline response. According to optical calculations, the light yield of double clad fibers should be 70% greater than that of similar single clad fibers. When one accounts for this effect, one finds a hypothetical double clad BCF-91A fiber will have a response of $1.7 \times 72\% = 122\%$. If true, trying to manufacture double clad BCF-91A fiber might prove appropriate for some applications. We conducted fluorescence tests which show that the primary fluor in BCF-91A is identical to that in Y11 (K27), although we are unable to determine the concentration in BCF-91A. Since the fluor and fiber dimensions are identical, we ascribe the difference to either fluor concentration or different manufacturing techniques for the two vendors.

Not surprisingly, the **Black extruded** option has low light yield. The light does not survive many bounces in the scintillator and is not trapped in the fiber. Similarly **3HF** has low light yield. This is understood by considering the light absorption spectrum of 3HF, which is peaked in the ultraviolet. Therefore the spectral matching between the 3HF and the blue emitting BC-404BL scintillator is poor.

5.5 Variation in Response Due to Fabrication

It is expected that different strips may give unequal number of photons in response to equal stimuli due to fabrication errors. Because each of the variations can have noticeably different responses, each must be treated separately. On the other hand, being able to combine results for all strips, in order to improve statistics, is appealing. What one can do is take the signal for each strip and divide it by the mean response of that particular configuration. The result is the normalized signal for each strip and the width of the normalized signal distribution gives a measure of the manufacturing non-uniformity. Such a distribution was made using the photon signal for all strips except for **3HF** (insufficient signal), **Black extruded** (insufficient signal) and **Clear extruded** (large edge effects).

The width of the resultant distribution is 7%. Variations in the quantum efficiency from the VLPCs will contribute to this width, as well as manufacturing non-uniformities. When the variation in VLPC effective QE is corrected, a 5% systematic error remains. This would imply that the contribution from the manufacturing non-uniformities is small.

Of the 112 strips used to evaluate manufacturing uniformity, there are two strips that were substantially outside the range of normal response variation. These strips had a response that was $\sim 50\%$ of the norm for that detector type. Since the preshower prototype is still being used, no detector post-mortem has been performed to determine the cause. Question of cause aside, one can say

that the “bad channel” fraction for the first module built was $\sim 2\%$.

5.6 End Effects

For several reasons, it is important to know the detailed response near the end of the scintillator (i.e. where the WLS fibers exit the scintillator and also at the opposite end near where the fiber is silvered). The end response was explored by plotting the average number of photoelectrons as a function of z in fine samples near the end. This was done for all detector variations at both ends. The shape of the curve was similar for all variations and is given in Fig. 8. The shape is consistent with a step function convolved with a Gaussian resolution function with width σ_T . This σ_T has two independent components: σ due to end non-uniformity and σ_z , the resolution in track z position reported from the fiber tracker (3.0 mm). These contribute in quadrature to σ_T . The σ from each detector is tabulated in Table 1. Each detector variation includes two ends, and therefore there are two σ ’s that must be reported: σ_l is for the left side of the detector (the side where the WLS fibers exit the scintillator on their way to the clear fibers) and σ_r is for the right side of the detector (the side with the silvered fiber ends). Generally, one expects $\sigma_l < \sigma_r$ since it is impossible for light from the scintillator to enter the WLS fiber in the region covered with silver. The size of this region varied, but was typically 2 to 3 mm in length. The σ of the convolved Gaussian resolution function is just one way to characterize the falloff in light yield near the ends. An additional useful piece of information is the distance from the end of the scintillator to a position where the light response is some fraction of the “normal” response. In order to determine a useful number, we calculate the distance between positions having 10% and 90% of the “normal” response; this distance varies with the detector configuration, but is typically 12 to 16 mm.

5.7 Crosstalk

Crosstalk occurs when a signal in a particular channel induces a spurious signal in an adjacent channel. In the case of the D \emptyset preshower prototype modules, two possible causes of crosstalk can be imagined: electrical and optical.

Since electrical crosstalk is observed to be small [19], the primary concern is optical. There are three possible mechanisms for light sharing between adjacent cells. The first is light tunnelling through the isolation glue separating the strips. The thickness of this glue is ~ 0.8 mm, and from visual inspection, it looks quite opaque and seems unlikely to contribute much to the overall crosstalk.

A second, substantially more likely, cause of optical crosstalk is light transported through the small amount of scintillator at the bottom of each isolation groove (see Fig. 2). Light is emitted along a track as a particle traverses the scintillator. Since the probability that a particular blue photon will hit the wavelength-shifting fiber without first bouncing off a scintillator surface is very small, the blue photons make many bounces before they pass into the WLS fiber and are absorbed. Although the top and bottom surfaces of the scintillators in the megatile options are smooth and the photons are reflected in a specular manner, the sides are quite rough and this diffuse reflection thoroughly randomizes the photons' directions. This randomization breaks up channelling effects and thus one expects the fraction of crosstalk between adjacent strips to be the ratio of the thickness of the scintillator underneath the isolation groove (nominally 0.015" (0.4 mm)) to the total scintillator thickness (nominally 0.177" (4.5 mm)). So the fractional crosstalk between adjacent cells from this effect is expected to be $(0.4/4.5) \sim 9\%$.

The final possible cause of crosstalk involves blue photons which exit the scintillator, bounce off the Tyvek wrapping over the isolation glue, and are reflected back into an adjacent strip. The amount of crosstalk from this cause is difficult to calculate, since poorly measured quantities come into play (e.g. reflectivity of the Tyvek, distance between the scintillator and Tyvek, etc.). However, this effect should somewhat increase the overall crosstalk.

Naively, crosstalk is an easy thing to measure. The signal in the central strip is taken to be the independent variable (X), the signal in an adjacent strip is taken to be the dependent variable (Y), and the mean Y ($\langle Y \rangle$) is plotted as a function of X . Our dominant crosstalk mechanism suggests that a simple linear function should describe the data. However, as seen in Fig. 9, a simple linear behavior is not observed.

The cause of the observed behavior is treated in some detail elsewhere [20], but we describe it briefly here. The number of photoelectrons is a quantized and small-valued quantity. Since the number of photoelectrons in both the main and adjacent strip fluctuates independently according to Poisson statistics, the observed distribution should obey the relation:

$$\langle \sigma \rangle = k \frac{\int_0^\infty e^{-S} S^{\Sigma+1} f(S) dS}{\int_0^\infty e^{-S} S^\Sigma f(S) dS}, \quad (2)$$

where σ is the number of photoelectrons seen in an adjacent strip, Σ is the number of photoelectrons in the central strip, S and s are the “true” signals before Poisson smearing in the main and adjacent strips, respectively, $k = s/S$ is the crosstalk fraction, and $f(S)$ is the distribution of true signals S . One should interpret this parameter k with care. It is the ratio of signals in the adjacent and central strip, not the fraction of total signal seen in the adjacent

strip.

As discussed in Ref. [20], it is imperative to know the underlying light yield distribution, $f(S)$, which is smeared by Poisson photostatistics into the observed distribution, $(\mathcal{F}(\Sigma))$ (cf. Fig. 7). The underlying light yield distribution should be proportional to the Landau fluctuation in energy loss rate dE/dx .

A Landau distribution was smeared according to Poisson statistics and the important parameters tuned until the yield distribution of Fig. 7 was reproduced. Then a function of the form suggested by Eq. (2) was evaluated. This function has only one free parameter (k), which was adjusted until the data of Fig. 9 were reproduced. It is expected that all of the megatile variations should have similar crosstalk, with the exception of the **Black Stripe** variation. When one analyzes all the detector variations, one finds that most are very similar, with a crosstalk fraction $k = (12 \pm 1)\%$. As expected, the **Black Stripe** variation has less crosstalk; $k = (4 \pm 0.5)\%$. However, there are two variations with crosstalk behavior distinctly different from the norm. **Optical Glue** has a crosstalk constant $k = (10 \pm 1)\%$, and **BC-404B Normal** has a crosstalk constant $k = (14.5 \pm 1)\%$. It is uncertain if these deviations are significant or if they reflect an as yet not understood systematic error.

In the preceding discussion we have required all tracks to be within 1.8 mm of the center of the main strip, a region where we expect k to be fairly constant. The fractional amount of signal in an adjacent strip increases when a track passes very near the edge of the central strip. In Fig. 10 we show the average amount of number of photoelectrons in the left adjacent strip as a function of the distance of the track from the main strip's center. (Note: there are typically two strips adjacent to a central strip. In this plot we are choosing an arbitrary side and looking at the crosstalk into strips on that side only.) Two curves are seen, one with substantially more crosstalk than the other. The curve with more crosstalk denotes the **BC-404B Normal** variation, while the lower crosstalk curve denotes the **Black Stripe** variant. While both curves show an asymmetry in the crosstalk curves, the asymmetry for the **Black Stripe** variant is much larger, even though the overall crosstalk is less. For the **Black Stripe** variant, the near side crosstalk is 16% above the mean, while the far side crosstalk is 16% below the mean. Thus for the **Black Stripe** variation, the near side crosstalk is 5.2% and that for the far side is 3.9%. For the other megatile variations, the asymmetries fall in the range of $(4.5 \pm 1.2)\%$.

Figure 10 shows a structure in the crosstalk signal similar to that seen in the main strip signal (see Fig. 6). This underscores the fact that the crosstalk signal is related to the amount of scintillator traversed by the charged particle (and therefore light produced). This can be further demonstrated if one plots the ratio $K = (\text{adjacent strip photoelectrons})/(\text{main strip photoelectrons})$ as a function of the distance of the track from the main strip's center. This ratio

K is very similar to the k discussed in the text surrounding Eq. (2) except it is the ratio of observed photoelectrons and not scintillator light. As shown in Fig. 11, the average amount of crosstalk into an adjacent strip is quite constant in the region $|\Delta x| < 1.8$ mm. The increase in the ratio K for $|\Delta x| > 1.8$ mm is explained because the number of photoelectrons in both the main strip and the adjacent strip are decreasing in this region (see Figs. 6 and 10). Because the number of photoelectrons is a quantized variable which is small in this region for both strips, the ratio of the two must go up. The asymmetry discussed above is clearly evident and reflects the fact that only crosstalk into the left adjacent strip is considered.

Crosstalk is observed in the various extrusion configurations as well. For the **Clear Extruded** variant, the crosstalk constant k is approximately 33%, underscoring the need for optical isolation. The **White Extruded** and **Normal Extruded** variations have crosstalk constants comparable to those seen in the megatile variations. We speculate that this is due to inadequate painting and intend to explore this conjecture in a subsequent prototype which will more thoroughly investigate the extrusion technologies.

6 Summary of Results

We have presented detailed data on the optical and scintillation properties of a plastic scintillating strip with wavelength shifting fiber and VLPC readout. Strips were (4.5×5.0) mm rectangular in cross section and one meter in length. The wavelength shifting fiber was silvered on one end and read out on the other end. The VLPC readout gave greatly improved photostatistics; typical light yields were 18 photons (and 4.5 photoelectrons) per mm of scintillator for cosmic rays with minimum energies of 2.5 GeV. With the thickness of scintillator used, each minimum ionizing particle typically yielded an average of 72 photons, which corresponds to 20 photoelectrons, given our readout system. Since the minimum number of photoelectrons needed is determined by the minimum allowed efficiency, this is four times what is required to efficiently see minimum ionizing particles. With this substantial light yield we were able to study attenuation length, signal uniformity, end effects, and crosstalk between strips in more detail than has been possible previously. Small variations in detector fabrication were tested and results were obtained for 14 megatile variations and four extrusion variations. Further tests with extruded scintillator and with triangular strip cross sections are planned in the near future.

Acknowledgement

The DØ Central Preshower group would like to thank a number of people for their substantial contributions to our work. The Fermilab Particle Detector group provided extruded scintillating strips for us to test. The people at Fermilab Lab 8 cut the megatiles for us, with special thanks going to Phyllis Deering and Scott Carlson. The DØ Mechanical Shop was very helpful in manufacturing the holder. The DØ Fiber Tracker Group very kindly provided us the use of their superb test stand. Julius Solomon provided us with tracking software and Jadwiga Warchol aided in the nonlinearity characterization. Finally, we would like to thank the DØ management, the U.S. Department of Energy and the U.S. National Science Foundation for their substantial support.

References

- [1] R. Wojcik et al., Nucl. Instr. and Meth. A 342 (1994) 416; Proceedings of SCIFI93: Workshop on Scintillating Fiber Detectors, ed. A.D. Bross, R.C. Ruchti, M.R. Wayne, World Scientific Press.
- [2] G. Apollinari et al., *CDF end plug calorimeter upgrade project*, University of Rochester preprint UR-1329, published in the proceedings of the IV International Conference on the Calorimetry in the High Energy Physics, La Biodola, Elba, Sep 19-25, 1993; G. Apollinari et al., Nucl. Instr. and Meth. A 324 (1993) 475.
- [3] D. Adams et al., FERMILAB-Conf-94/318-E, presented at DPF'94; M. Atac et al., Nucl. Instr. and Meth. A 314 (1992) 56; M.D. Petroff and M.G. Stapelblock, IEEE Trans. Nucl. Sci. **NS-36** (1989) 158; M.D. Petroff and M. Atac, *ibid.*, p. 163.
- [4] B. Gomez et al., (DØ Collaboration), FERMILAB-DØUPGRADE-E-823, Oct 1993.
- [5] The DØ Central Preshower Group, *The Central Preshower Detector for the DØ Run II Upgrade*, DØ note #2137 (available from the authors).
- [6] S. Abachi et al., Nucl. Instr. and Meth. A 338 (1994) 185; S. Aronson et al., Nucl. Instr. and Meth. A269 (1988) 492.
- [7] D. Adams et al., FERMILAB-Conf-94/312-E, presented at DPF'94; DØ Fiber Tracking Group, *Cosmic Ray Test Results of the DØ Prototype Scintillating Fiber Tracker*, to be published in the proceedings of the 4th International Conference on Advanced Technology and Particle Physics, Como, Italy, 3-7 October 1994, Ed. by Z. Borchi.
- [8] Kuraray Intl., 200 Park Ave, New York, NY 10166, USA. Tel. +1 (212) 986-2230.
- [9] A. Pla-Dalmau, A.D. Bross, and C.W. Spangler, FERMILAB-Pub-93/038, Submitted to Journal of the Chemical Society Perkin Transactions 2; A.D. Bross, A. Pla-Dalmau and C.W. Spangler, Nucl. Instr. and Meth. A 325 (1993) 168; A.D. Bross et al., Nucl. Instr. and Meth. A 307 (1991) 35; A.D. Bross and A. Pla-Dalmau, Nucl. Instr. and Meth. A 327 (1993) 337.
- [10] Bicron Corporation, 12345 Kinsman Road, Newbury, OH, 44065-9677, USA. Tel. +1 (216) 564-2251.
- [11] M. Kusner, B. Harter, K. Blackman, Bicron Corporation, private communication.
- [12] A. Pla-Dalmau, G.W. Foster and G. Zhang, Volume 1, FERMILAB-TM-1873, December 1993; A. Pla-Dalmau, G.W. Foster and G. Zhang, FERMILAB-TM-1875, December 1993.

- [13] T. Hasegawa et al., Nucl. Instr. and Meth. A 311 (1992) 498.
- [14] See especially: M. Olsson, et al., University of Rochester Preprint UR-1370 ER-40685-920, Aug 1994. See also, P. de Barbaro et al., UR-1371, Sep 1994; P. de Barbaro, et al., UR-1398, Jan 1995, submitted to IEEE Trans. Nucl. Sci.
- [15] Type 1073D Tyvek, DuPont Fibers, Chestnut Run Plaza, P.O. Box 80705, Wilmington, DE 19880, USA.
- [16] S. Margulies and M. Chung, in “Scintillating Fiber Technology and Applications II”, ed. E. J. Fenyves, Proc. SPIE, Vol. 2281, pp. 26-34, 1994.
- [17] J. Thompson, private communication, Nucl. Instr. and Meth. A article in preparation.
- [18] C.L. Kim, private communication, Nucl. Instr. and Meth. A article in preparation.
- [19] J. Warchol, private communication.
- [20] D. Lincoln, F. Hsieh, H. Li, University of Michigan Preprint UM HE 95-03 March 1995, to be published in Nucl. Instr. and Meth. A.

Figure Captions

1. An end view schematic of the DØ Fiber Tracking Group’s cosmic ray tracker. The four black boxes labelled “Trigger Counters and Chambers” represent both the trigger counters and the Iarocci chambers, except for the bottom one, where only a trigger counter is present. The preshower prototype is nestled under the fiber tracker. The distance from top to bottom is about 3 meters. The figure is not to scale.
2. Shown are the construction details of the “normal” megatile design. Both isolation and fiber grooves are shown. Note that the layer-to-layer staggering is half a cell.
3. This plot illustrates the impressive performance of the VLPC. The 0, 1, 2 and 3 photoelectron peaks can be seen.
4. This plot shows typical nonlinearity curves in the electronics chain from amplifier to ADC. Generally, the response of the amplifier is linear until about 20 photoelectrons, at which point the response quickly becomes nonlinear. The various channels are substantially similar. For any particular number of ADC counts, the channel-to-channel spread in the corresponding number of photoelectrons is about 10%. Each channel is linearized separately.
5. Shown are the attenuation curves for the cases of silvered and unsilvered WLS fibers. The response of silvered fibers is given by the circles, while the typical response for unsilvered fibers is drawn in as a line and is labeled “Direct”. The silvered fiber case has a small attenuation loss over the entire meter of scintillator. The unsilvered case shows noticeably more loss. Fluctuations around the average trend are on the order of 2-3%, with some points varying as much as 7-8%. In addition, both the direct light component (which is equivalent to the unsilvered case) and reflected light component are indicated. The unsilvered attenuation length used is $\lambda = 4.5$ m, with a reflection coefficient $R = 0.7$. These data correspond to the **0.050”** detector variation.
6. Shown is the signal uniformity across the strip for three different fiber groove depths. The vertical lines at $\pm(0.05, 0.21, 0.25)$ cm correspond to the edges of the fiber groove, the scintillator/glue interface, and the center of the isolation glue, respectively. It is apparent that the depth of the dip in light yield is related to the depth of the fiber groove. The slight asymmetry in the location of the central groove is understood to be due to a $100 \mu\text{m}$ shift in putting the scintillator back on the milling table. Note that the vertical axis is given in number of photoelectrons. Each detector variant is attached to VLPC’s with different quantum efficiencies (see Sec. (5.4)).
7. Shown is a typical yield curve. The horizontal axis is the number of photoelectrons per millimeter of scintillator traversed. Only data in the region of maximum light yield are used (i.e. $|\Delta x| < 0.05$ cm and $|\Delta x| > 0.15$ cm are excluded, where Δx is the distance between the center of the strip and the track intercept at the strip, halfway between the top and bottom surfaces). The signal is clearly separate from pedestal. This particular plot

corresponds to the **0.100"** variation.

8. Shown is the response of the detector (in average number of photoelectrons) for particles near the end of the detector. For this plot, there is no restriction on where the particles can hit the strip, other than the restriction that they must be within 2.5 mm of the strip center in x . The result shown here is for **404B Normal**.
9. Shown is the crosstalk for two detector variations. The solid circles are for **BC-404B Normal**, the open squares are for **Black Stripe**. In both cases, the horizontal axis is the number of photoelectrons seen in the “central” strip. The vertical axis is the average number of photoelectrons seen in an adjacent strip. When applicable, both adjacent strips are used and thus often there are two entries per central strip in this plot. In order to avoid non-uniformities in the amount of crosstalk for different parts of the strip (especially near the edges), a cut of $|\Delta x| < 1.8$ mm is imposed, where Δx is the distance between the center of the strip and the track intercept at the strip, halfway between the top and bottom surfaces. As expected, **Black Stripe** has less crosstalk than **BC-404B Normal**. The “dual slope” nature of the curves is discussed in the text.
10. Shown is the amount of crosstalk in a neighboring strip as a function of the position of a track with respect to the center of the central strip. On the vertical axis is plotted the average number of photoelectrons seen in the adjacent strip to the left of the central strip. The adjacent strip to the right of the central strip is not included in this plot. The horizontal axis is the distance of the track from the center of the central strip, in units of centimeters. The open squares are for the **Black Stripe** variation. The solid circles are for the **BC-404B Normal** variation.
11. Shown is the ratio K which is the number of photoelectrons in an adjacent strip divided by the number of photoelectrons in the hit strip as a function of the track position in the hit strip. In this plot only crosstalk into the left adjacent strip is included. The horizontal axis is the distance of the track from the center of the central strip, in units of centimeters. The open squares are for the **Black Stripe** variation. The solid circles are for the **BC-404B Normal** variation.

Detector Variation	R	σ_r (mm)	σ_l (mm)
0.100”	0.59±0.01	4.70 ± 0.46	4.91 ± 0.43
0.050”	0.88±0.01	4.27 ± 0.35	3.32 ± 0.34
404B Normal	0.81±0.01	4.74 ± 0.46	2.77 ± 0.29
404A Normal	0.82±0.01	5.44 ± 0.31	4.05 ± 0.42
404B Heated	0.79±0.01	4.05 ± 0.36	3.12 ± 0.38
404A Heated	0.82±0.01	3.60 ± 0.33	4.01 ± 0.49
404B Crazed	0.79±0.01	4.23 ± 0.35	3.07 ± 0.34
404A Crazed	0.84±0.01	5.24 ± 0.38	4.01 ± 0.44
0.038”	0.81±0.01	4.57 ± 0.31	2.87 ± 0.29
Black Stripe	0.81±0.01	4.23 ± 0.35	3.17 ± 0.42
Optical Glue	0.77±0.01	5.72 ± 0.35	3.12 ± 0.31
BCF-91A	0.81±0.01	4.99 ± 0.35	3.22 ± 0.32
Y11 350	0.81±0.01	4.82 ± 0.35	2.97 ± 0.32
Normal Extruded	0.92±0.01	5.72 ± 0.49	4.53 ± 0.36
Clear Extruded	0.93±0.01	4.27 ± 0.32	4.53 ± 0.44
White Extruded	0.92±0.01	3.96 ± 0.52	5.03 ± 0.45

Table 1

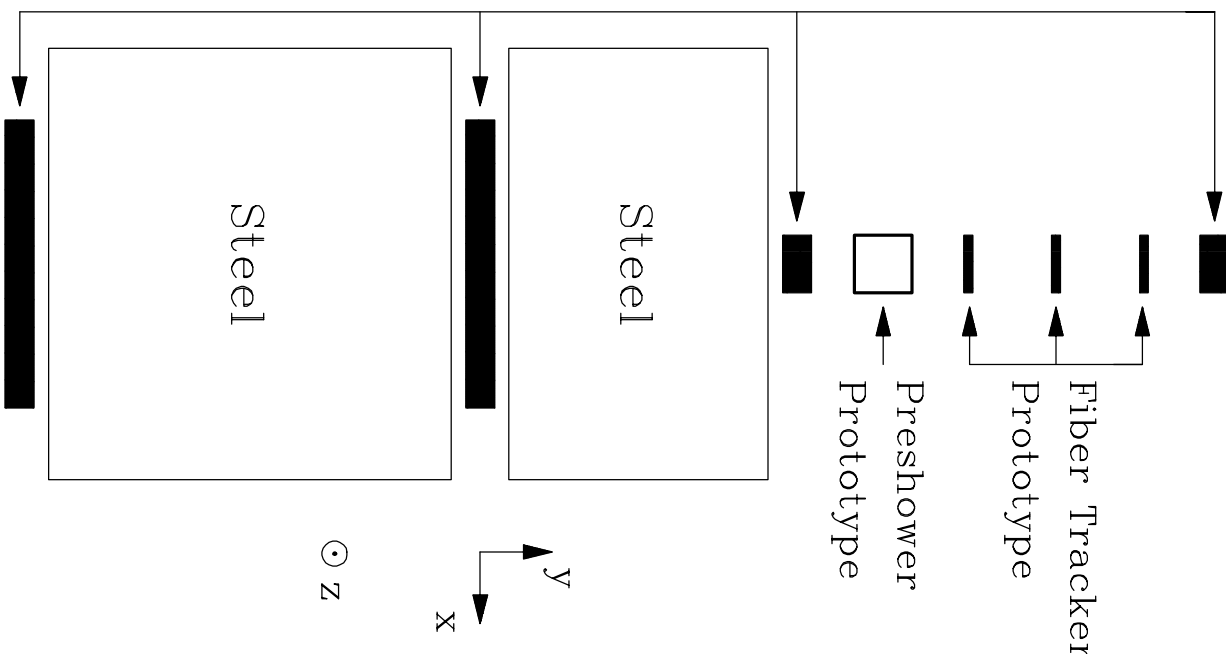
R is the ratio of the average response of particles travelling through the fiber groove to average response of particles travelling through the part of the strip that gives maximum signal. Detectors are grouped by “like” construction techniques. As expected, R is related to the depth of the fiber groove. There appears to be a degree of uniformity between “like” construction techniques. Also shown is the width (in mm) of the region of reduced light yield at the ends of the scintillators. σ_l denotes the end of the scintillator where the WLS fibers exit the strip. σ_r denotes the end with the silvered end of the fiber. Details of the definitions are given in the text.

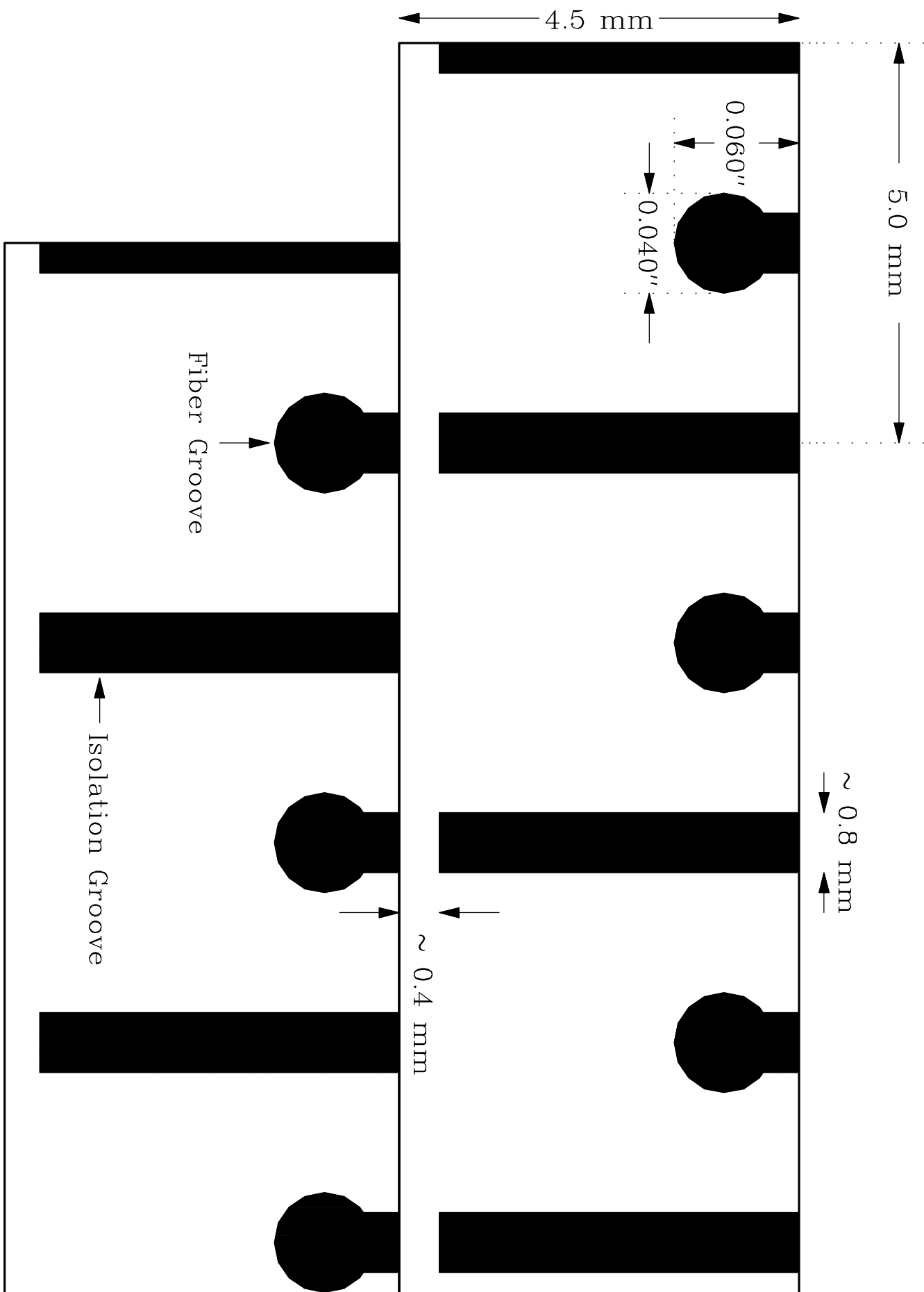
Detector Variation	Mean (pe/mm)	RMS (pe/mm)	# Events	Mean (Photons/mm)	Relative Response
	$\pm 2\%$	$\pm 2\%$		$\pm 20\%$	
Optical Glue	6.13	2.31	39965	24.94	133.1 ± 5.7
404B Normal	4.10	1.72	42823	18.74	100.0 ± 3.0
0.050”	4.36	1.85	40787	18.61	99.4 ± 4.5
0.038”	4.51	1.67	42067	17.96	95.8 ± 4.4
404B Heated	4.67	1.74	38792	17.83	95.2 ± 4.5
Y11 350	4.92	1.85	38575	17.62	94.1 ± 4.2
404A Normal	4.67	1.65	38471	17.33	92.5 ± 4.0
0.100”	5.15	2.05	36309	17.14	91.5 ± 4.1
404A Crazed	4.67	1.74	39649	15.86	84.7 ± 4.5
Black Stripe	4.38	1.97	38273	15.51	82.8 ± 3.6
404A Heated	4.51	1.65	35924	15.50	82.7 ± 3.9
404B Crazed	4.05	1.69	37712	14.62	78.0 ± 5.9
BCF-91A	3.85	1.54	42127	13.44	71.7 ± 3.0
Normal Extruded	3.16	1.38	18540	10.79	57.6 ± 2.5
White Extruded	2.98	1.26	21868	10.57	56.4 ± 2.5
Clear Extruded	2.10	0.96	16643	8.13	43.4 ± 3.1
Black Extruded	0.28	0.28	16198	0.85	4.5 ± 0.2
3HF	0.00	0.00	39317	0.00	0.0 ± 0.0

Table 2

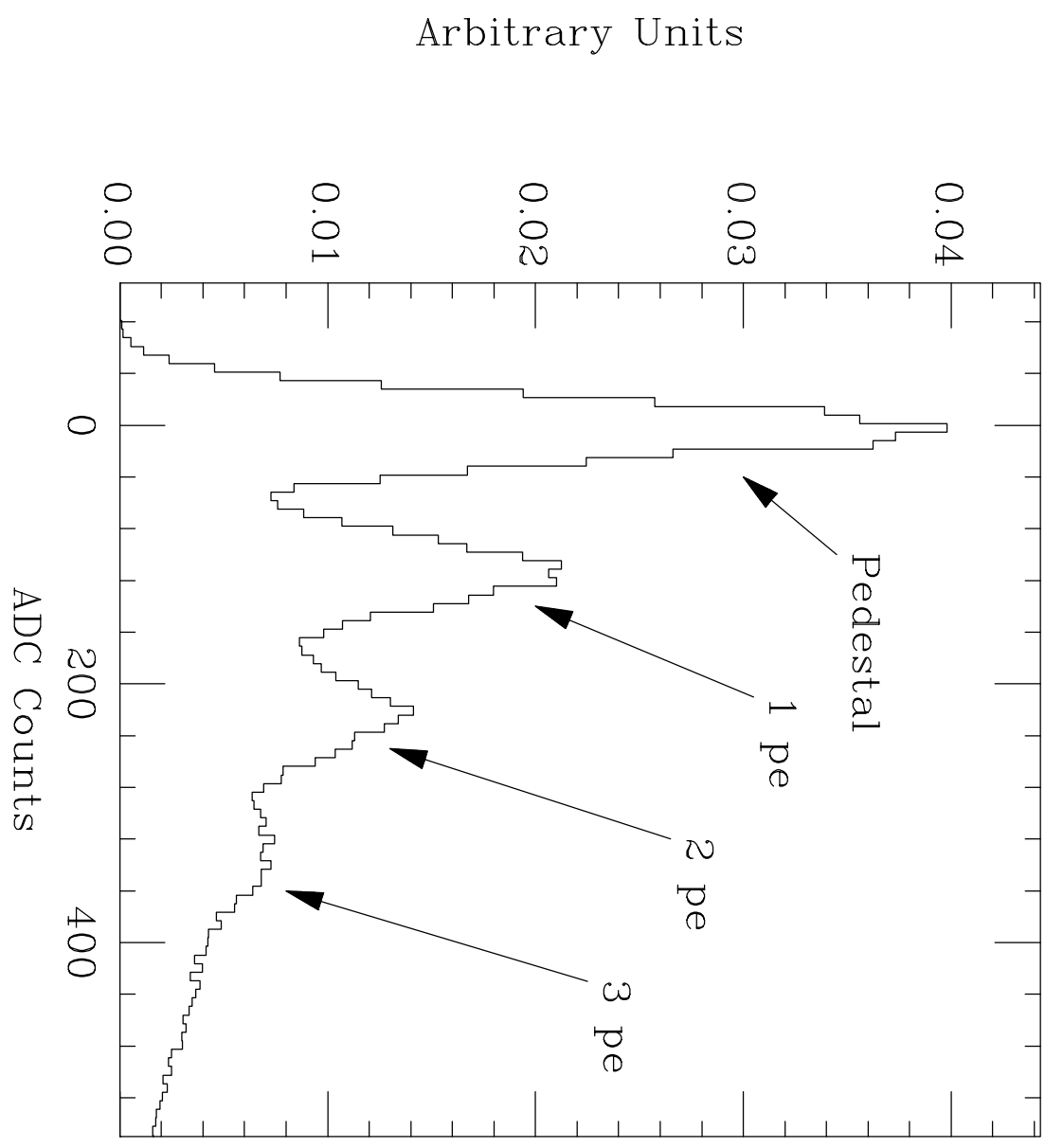
Tabulated are the responses of each detector variation in units of photoelectrons (and photons) per millimeter. While the results change if the most probable value is used rather than the mean (most probable $\sim 90\%$ of the mean), the relative response does not. The relative response compares the number of photons exiting each detector variant. Only data in the region of maximum light yield are used (i.e. $|\Delta x| < 0.05$ cm and $|\Delta x| > 0.15$ cm are excluded, where Δx is the distance between the center of the strip and the track intercept at the strip, halfway between the top and bottom surfaces).

Trigger Counters and Chambers

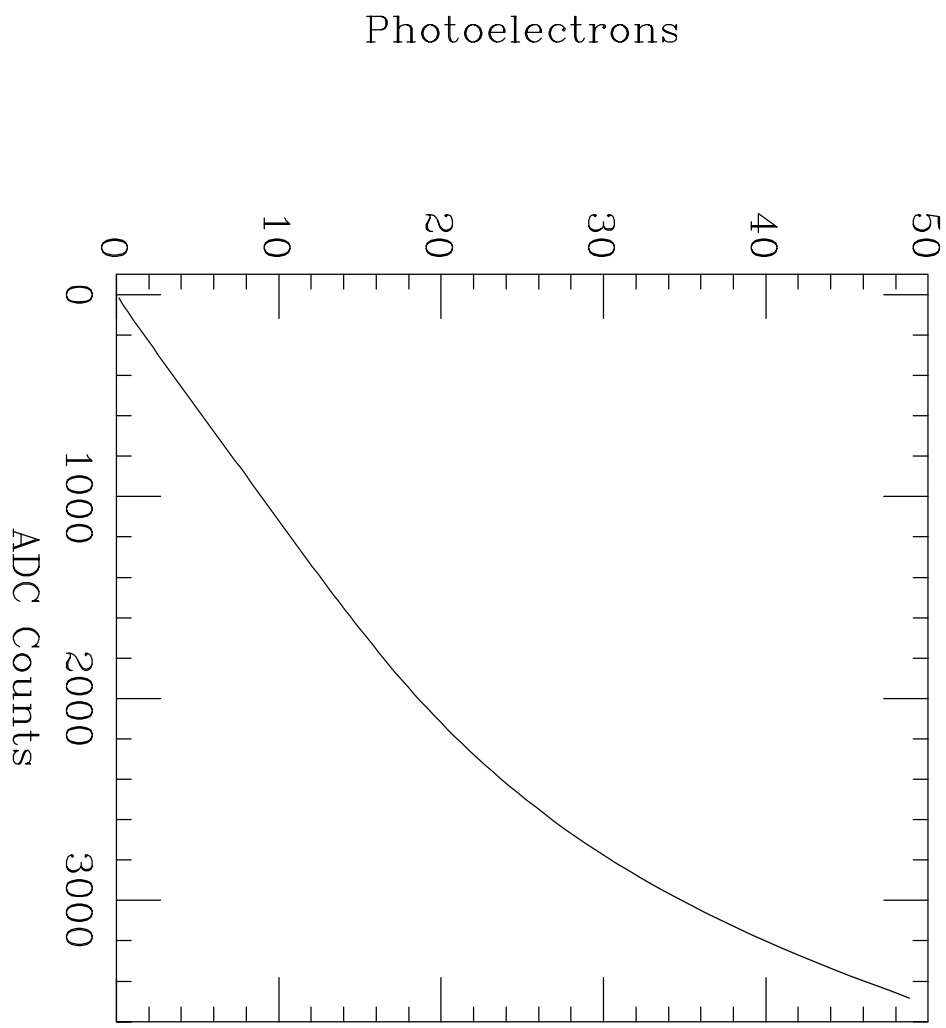




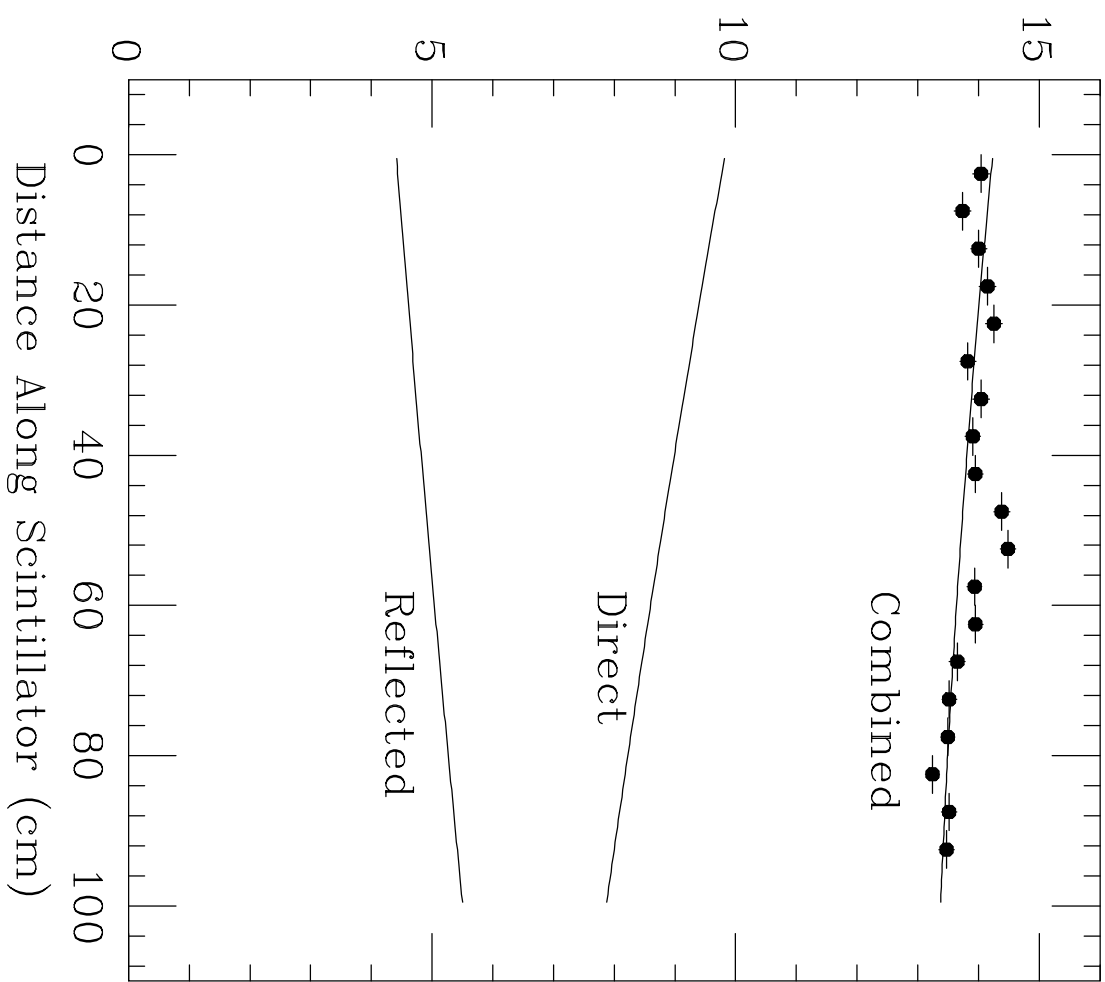
Individual Photoelectron Spectrum



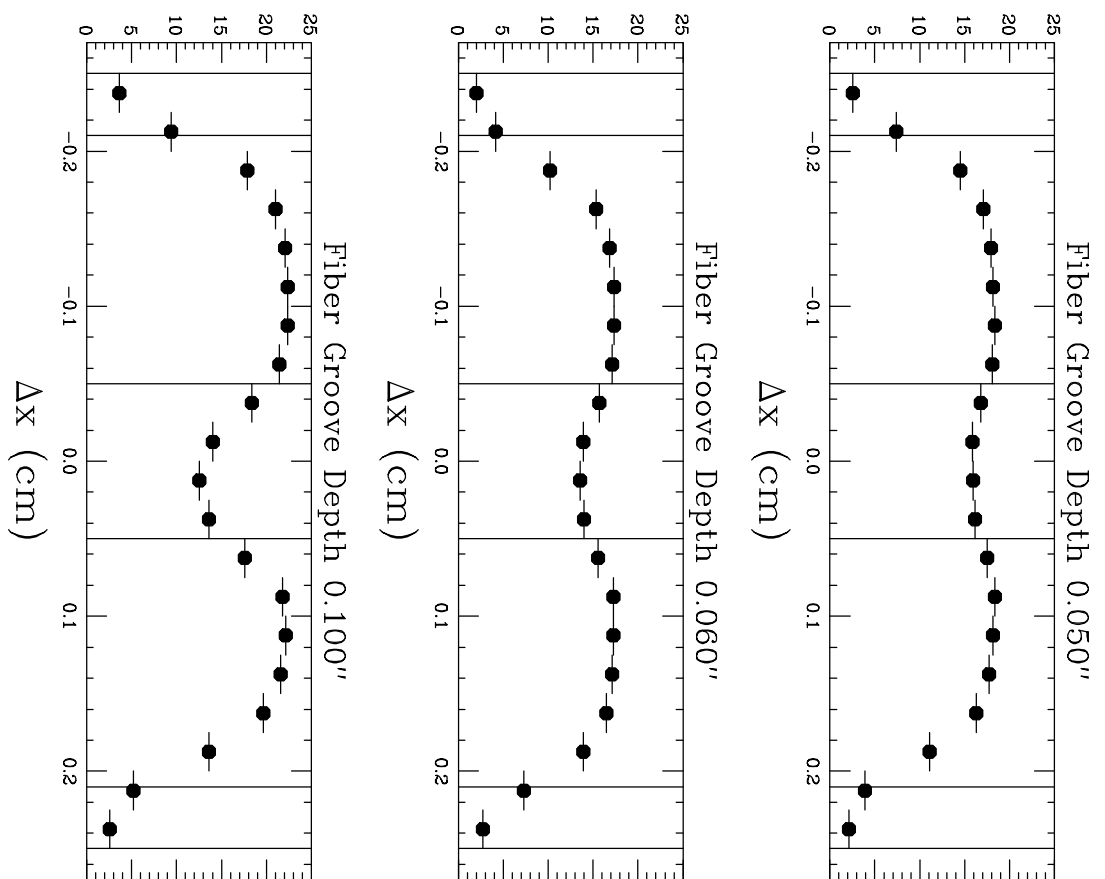
Typical Nonlinearity in Electronic Chain



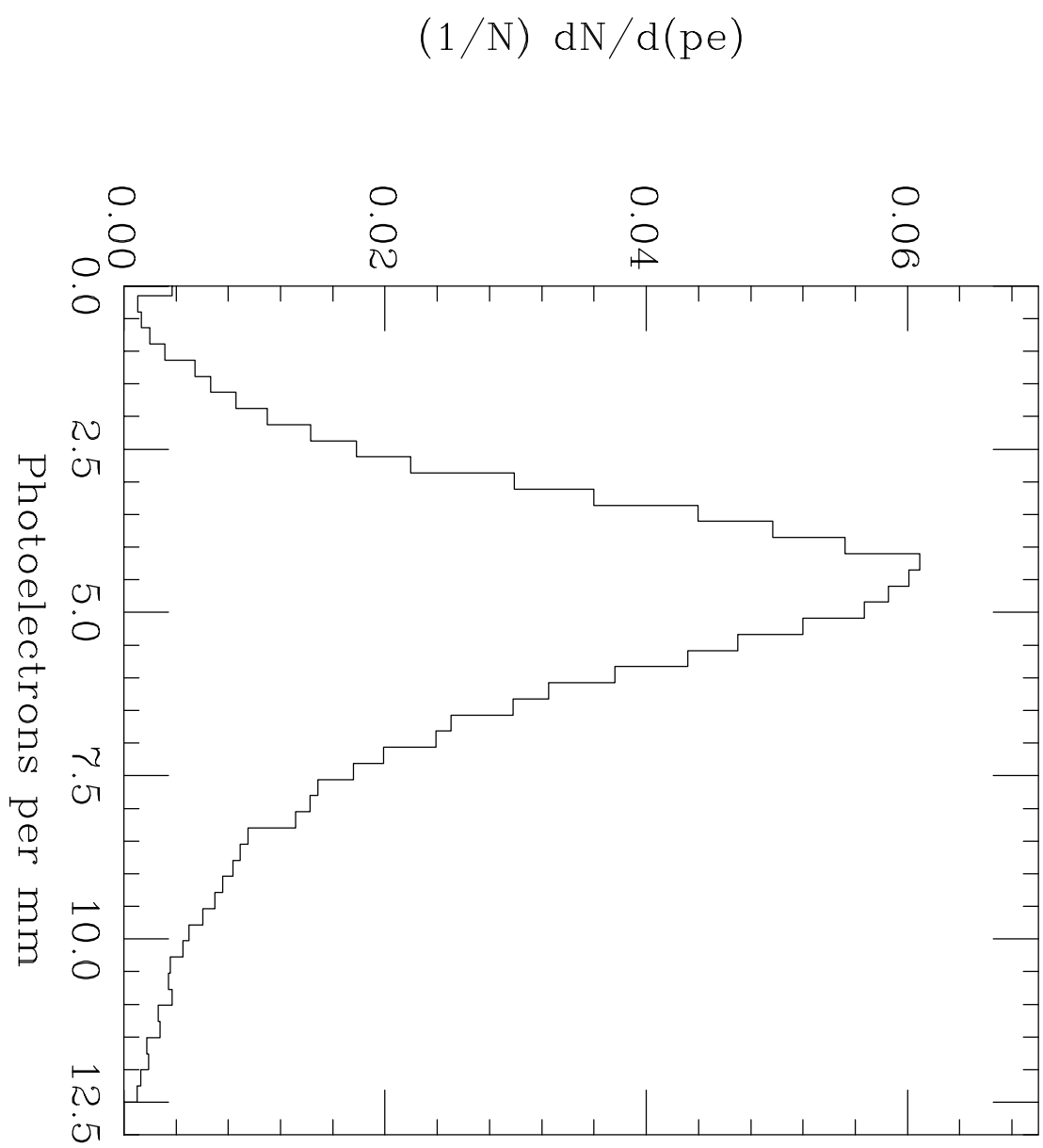
Typical Attenuation Curve



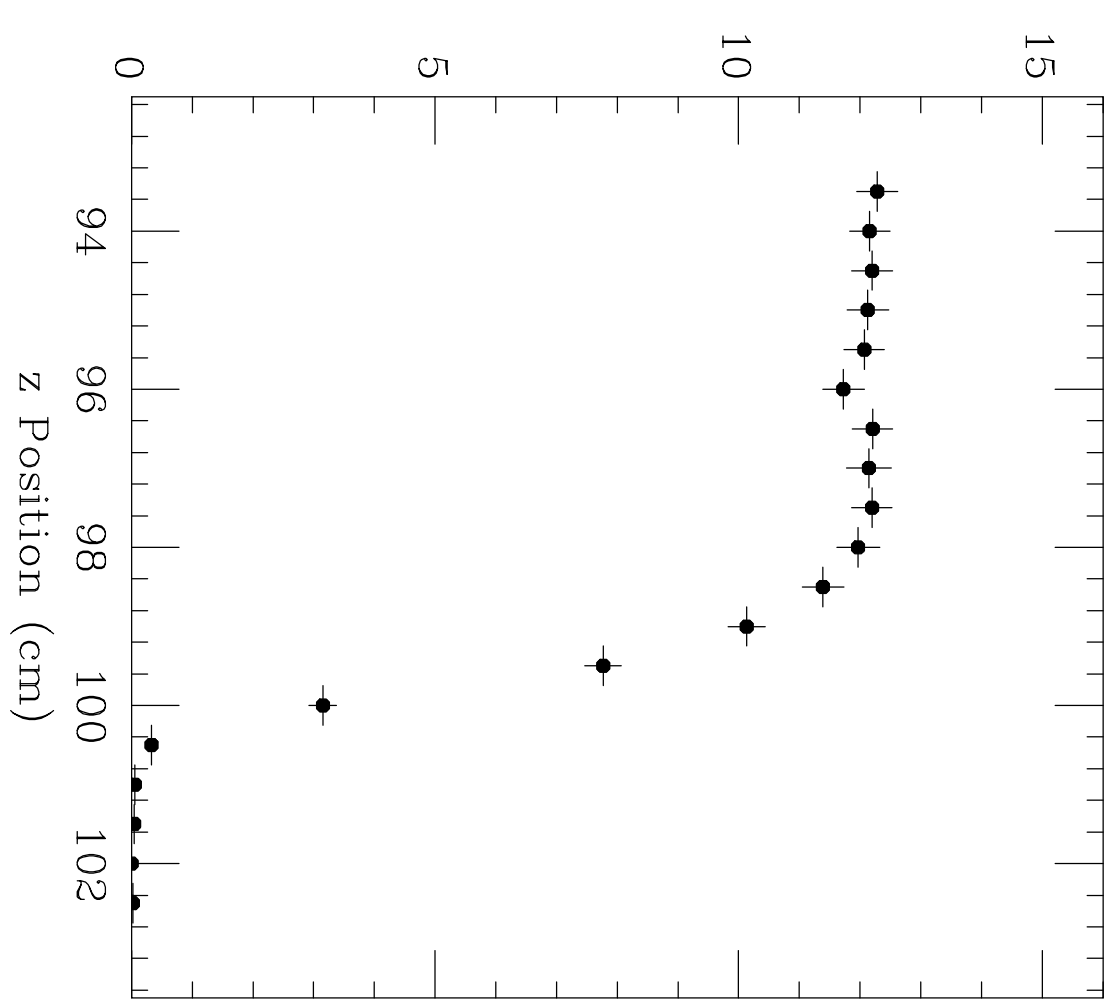
Average Number of Photoelectrons



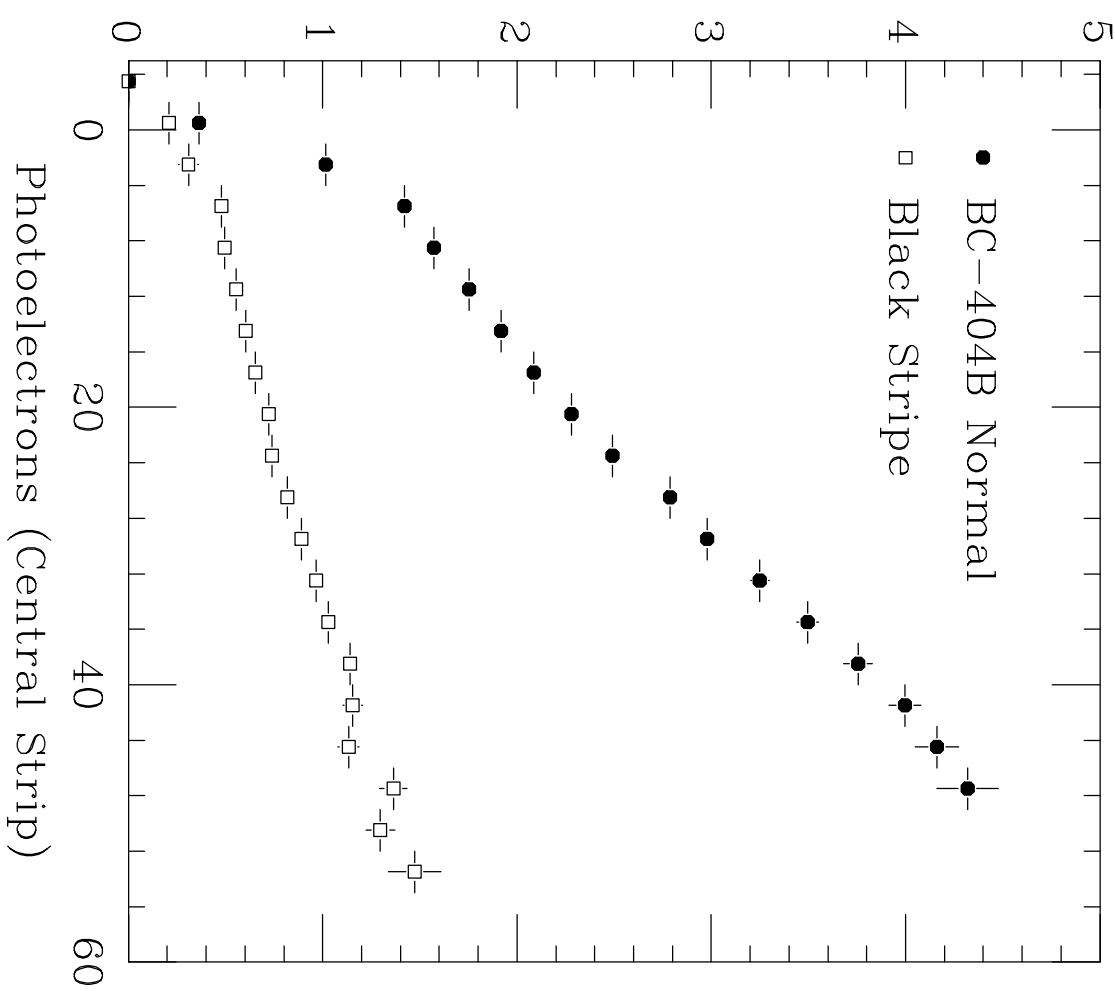
Typical Photoelectron Yield



Typical End Effect Curve



Typical Crosstalk Curves



Photoelectrons (Adjacent Strip)

Crosstalk Asymmetry

